



**HAL**  
open science

## Permeability evolution in variably glassy basaltic andesites measured under magmatic conditions

Alexandra Roma Larisa Kushnir, Caroline Martel, Rémi Champallier, F. B. Wadsworth

► **To cite this version:**

Alexandra Roma Larisa Kushnir, Caroline Martel, Rémi Champallier, F. B. Wadsworth. Permeability evolution in variably glassy basaltic andesites measured under magmatic conditions. *Geophysical Research Letters*, 2017, 44, pp.10,262-10,271. 10.1002/2017GL074042 . insu-01622091

**HAL Id: insu-01622091**

**<https://insu.hal.science/insu-01622091>**

Submitted on 16 Nov 2017

**HAL** is a multi-disciplinary open access archive for the deposit and dissemination of scientific research documents, whether they are published or not. The documents may come from teaching and research institutions in France or abroad, or from public or private research centers.

L'archive ouverte pluridisciplinaire **HAL**, est destinée au dépôt et à la diffusion de documents scientifiques de niveau recherche, publiés ou non, émanant des établissements d'enseignement et de recherche français ou étrangers, des laboratoires publics ou privés.



## RESEARCH LETTER

10.1002/2017GL074042

## Key Points:

- High-temperature permeability measurements must be corrected for the role of temperature on the density of the pore fluid
- Permeability of glassy volcanic rocks is sensitive to changes in temperature above the glass transition
- Permeability changes very little in glass-poor volcanic rocks up to high temperature

## Supporting Information:

- Supporting Information S1

## Correspondence to:

A. R. L. Kushnir,  
alexandra.kushnir@gmail.com

## Citation:

Kushnir, A. R. L., Martel, C., Champallier, R., & Wadsworth, F. B. (2017). Permeability evolution in variably glassy basaltic andesites measured under magmatic conditions. *Geophysical Research Letters*, 44. <https://doi.org/10.1002/2017GL074042>

Received 3 MAY 2017

Accepted 8 OCT 2017

Accepted article online 12 OCT 2017

## Permeability Evolution in Variably Glassy Basaltic Andesites Measured Under Magmatic Conditions

A. R. L. Kushnir<sup>1,2</sup> , C. Martel<sup>1</sup>, R. Champallier<sup>1</sup> , and F. B. Wadsworth<sup>3</sup> 

<sup>1</sup>Institut des Sciences de la Terre d'Orléans (ISTO), UMR 7327-CNRS/Université d'Orléans/BRGM, Orléans, France, <sup>2</sup>Institut de Physique du Globe de Strasbourg (IPGS), UMR 7516-CNRS/Université de Strasbourg, Strasbourg, France, <sup>3</sup>Department for Earth and Environmental Sciences, Ludwig-Maximilians-Universität, Munich, Germany

**Abstract** Heat from inflowing magma may act to seal permeable networks that assist passive outgassing at volcanic conduit margins and in overlying domes, reducing the efficiency of overpressure dissipation. Here we present a study of the evolution of permeability—measured under magmatic conditions—with increasing temperature in glassy and glass-poor basaltic andesites from Merapi volcano (Indonesia). Whereas the permeability of glass-poor rocks decreases little up to a temperature of 1,010°C, glassy specimens experience a pronounced decrease in permeability above the glass transition once the viscosity of the crystal suspension is low enough to relax under external stresses. Changes in temperature alone are thus not enough to significantly modify the permeability of the glass-poor rocks that commonly form Merapi's dome. However, the presence of glass-rich domains in a dome may lead to local sealing of the volcanic plumbing between eruptions, exacerbating localized overpressure development that could contribute to explosivity.

### 1. Introduction

The precarious balance between overpressure development and dissipation in volcanic systems is one of the fundamental controls on eruption behavior (Eichelberger et al., 1986; Jaupart & Allegre, 1991; Mueller et al., 2008; Rust et al., 2004; Woods & Koyaguchi, 1994). Volatiles can outgas when a permeable network develops by shear-induced bubble coalescence (Okumura et al., 2009, 2006, 2008) or magma fracture (Kushnir et al., 2017; Stasiuk et al., 1996; Tuffen & Dingwell, 2005). However, the efficiency of volatile release to the atmosphere depends on the time-dependent availability of preexisting outgassing pathways across conduit margins and through the edifice structure. Any impediment to gas escape via these avenues leads to an inevitable increase in pressure within the volcanic plumbing system, increasing the likelihood of an explosive response.

Volatiles often make their way to conduit margins where strain is localized (e.g., Gaunt et al., 2014; Rust et al., 2004; Thomas & Neuberg, 2012; Tuffen & Dingwell, 2005) and permeable networks can either siphon volatiles through the conduit walls (Heap et al., 2015; Jaupart, 1998) or direct them up along the conduit margins (Gaunt et al., 2014; Kushnir et al., 2017; Lavallée et al., 2013; Rust et al., 2004) and to the surface via the overlying edifice structure (Collinson & Neuberg, 2012; Collombet, 2009; Jaupart, 1998). The ability of the surrounding conduit wall rock to dissipate accumulated volatiles is dependent on the rock's structure, which may experience continued microstructural modification when exposed to temperatures that carry the amorphous phase of the rock above its glass transition (Kennedy et al., 2010; Schaubroth et al., 2016). Indeed, fluctuations in temperature at conduit margins can lead to shifting zones of rock compaction and viscous deformation that operate to limit permeability (Heap et al., 2017). In particular, because the stresses necessary to induce viscous deformation in melts are much smaller than those needed to compact volcanic rocks, the cessation of flow of magmatic volatiles may be more efficient at high temperatures (Heap et al., 2017) and result in overpressure development within the volcanic edifice.

The permeability of volcanic products has been extensively studied under ambient laboratory conditions (e.g., Bernard et al., 2007; Farquharson et al., 2015; Klug & Cashman, 1996; Kushnir et al., 2016; Rust & Cashman, 2004; Saar & Manga, 1999; Wright et al., 2009) and while such measurements can provide critical post mortem insight into the processes governing permeability creation and destruction, they only provide a snapshot of a moment in the structural evolution of volcanic materials. Further, the permeability of erupted volcanic products may be modified by postemplacement processes—for example, cooling (Gaunt et al., 2016; Vinciguerra et al., 2005), crystallization (Kushnir et al., 2016; Wright et al., 2011), and transport

(Siebert, 1984)—that play important roles in the upper edifice and dome but may be less appropriate in constraining fluid movement deeper within the conduit. Thus, the expansion of these studies to conditions appropriate to the middle- to lower-conduit requires the implementation of high temperature techniques. So-called in situ permeability measurements have been performed on granites (Moore et al., 1994; Morrow et al., 2001; Summers et al., 1978; Watanabe et al., 2017), amphibolites and gneisses (Zharikov et al., 2003), ophiolites (Coelho et al., 2015), limestone (Bakker et al., 2015; Fischer & Paterson, 1992), marble (Fischer & Paterson, 1992), sandstone (Fischer & Paterson, 1992), and glass-free dacites (Gaunt et al., 2016). However, to date, only one study has addressed the implications of permeability evolution with changing temperature on eruptive behavior, highlighting the competing micromechanisms that act to create and destroy permeable networks in volcanoes (Gaunt et al., 2016).

Here we consider the complexities of measuring permeability at high temperature under steady state flow conditions for glassy and glass-poor basaltic andesites from the 2010 eruption of Gunung Merapi (Indonesia). We explore the processes that modify the permeability of these materials as temperature is increased to 1,010°C under hydrostatic conditions and, subsequently, cooled to ambient laboratory conditions and the implications of these attendant processes on volcanic outgassing.

## 2. Permeability and Temperature

Permeability,  $k$ , is a fundamental rock property that is controlled by a material's void space microstructure. Darcy's law,  $Q_v = - (kA/\mu) \times (\partial P/\partial x)$ , is the constitutive equation used to describe the efficacy of fluid flow along some length,  $\partial x$ , of a permeable material under an applied differential pore fluid pressure,  $\partial P$ , where  $Q_v$  is the volumetric flow rate,  $\mu$  is the viscosity of the pore fluid, and  $A$  is the cross sectional area available for flow. Darcy's law assumes that (i) there is conservation of mass of the pore fluid along the sample, (ii) the temperatures of the sample and pore fluid are constant and equal to each other, and (iii) changes in sample microstructure occur over timescales longer than the time of observation. For a sample with a fixed length,  $L$ , and assuming steady state flow, permeability is

$$k = \frac{-\mu L Q_v}{A \Delta P}, \tag{1}$$

where  $\Delta P = P_d - P_u$  and  $P_u$  and  $P_d$  are the upstream and downstream pore fluid pressures, respectively. Equation (1) assumes that the pore fluid is incompressible. For a compressible pore fluid, permeability is calculated by

$$k = \frac{Q_v \mu L P_d}{A (P_u - P_d) P_m}, \tag{2}$$

where  $P_m = (P_u + P_d)/2$  is the mean pressure across the sample (see supporting information for a comprehensive derivation).

Equation (2) assumes that the temperatures in the pore fluid reservoirs upstream and downstream of the sample are equal to the sample temperature and remain constant throughout measurement. This assumption is not satisfied when the majority of the pore fluid volume resides outside a furnace, as is often the case when performing laboratory measurements (Bakker et al., 2015; Gaunt et al., 2016; Moore et al., 1994; Morrow et al., 1981, 2001; Zharikov et al., 2003). Therefore, the effect of temperature on the volumetric flow rate of the pore fluid must be considered before the effect of temperature on the sample permeability can be assessed.

To account for the change in volume induced by the temperature gradient between the sample (high temperature) and where volumetric flow is measured (room temperature), Morrow et al. (2001) calculate the flow rate through the heated sample:  $Q_T = Q_v (V_T/V_v)$ , where  $Q_T$  is the volumetric flow rate through the sample,  $Q_v$  is the flow rate measured at ambient laboratory temperature by the flow meter,  $V_T$  is the specific volume of the pore fluid at temperature  $T$ , and  $V_v$  is the specific volume of the pore fluid as it passes through the flow meter. This correction can be restated:

$$Q_T = Q_v \left( \frac{\rho_v}{\rho_T} \right) \tag{3}$$

where  $\rho_v$  and  $\rho_T$  are the density of the pore fluid at ambient laboratory temperature and the sample temperature, respectively. Therefore, the permeability of a sample at high temperature when measuring  $Q_v$  at ambient laboratory conditions is

$$k = \frac{Q_v \rho_v}{\rho_T} \frac{\mu_T L P_d}{A(P_u - P_d)P_m}, \quad (4)$$

where  $\mu_T$  is the viscosity of the pore fluid as it flows through the sample.

### 3. Methods

We measured permeability under hydrostatic conditions in an internally heated pressure vessel equipped with a pore fluid pressure system (see supporting information). In this study, both the confining medium and pore fluid were argon. Two volumetric flow rate meters measuring  $Q_v$  up to 1 or 300 mL/min, respectively, were installed in parallel at the sample outlet and operated at gas pressures below 2 MPa. The mean pore fluid pressure,  $P_m$ , never exceeded 1 MPa. For rock samples between 10 and 15 mm in diameter and 15 mm in length, this system can measure permeabilities between  $10^{-13}$  and  $10^{-19}$  m<sup>2</sup>.

All samples were jacketed in iron sleeves, effectively separating the pore fluid from the confining medium. At high temperature (above 380°C, see supporting information), the strength of the iron jacket is low (Frost & Ashby, 1982) and the jacket molds to the sample shape, creating an effective seal between the inside of the jacket and the sample sides. To avoid jacket punctures and leaks, all rock samples were cored to 10 mm diameter and placed in 2.5 mm thick Teflon (for  $T < 400^\circ\text{C}$ ; see supporting information) or copper (for  $T \geq 400^\circ\text{C}$ ) sleeves, which were subsequently mounted in iron-jacketed sample assemblies.

Permeable ceramic spacers were placed on either end of the samples, ensuring that the pore fluid impinged uniformly on the entire sample end. We note that while we could monitor the fluid flow ( $Q_v$ ) through all samples, two of the rocks (HT-2 and HT-3; Table S1) were more permeable than the ceramic spacers and we could not determine their permeabilities. To mitigate the influence of the ceramic spacers on the permeability measurements, we drilled 4 mm diameter holes into the spacers to ensure that they did not act as bottlenecks to flow.

Samples were heated at 10°C/min to each target temperature and the microstructure was allowed to equilibrate for 1 h before permeability was measured; the time allowed for sample equilibration and measurement did not exceed 2 h for any given temperature step. The sample temperature was monitored using an N-type thermocouple placed 3 mm above the sample, and the temperature did not vary by more than 2°C across the sample length. The temperature profile along the entire furnace length (Figure S2) did not vary by more than 24°C between the sample position and furnace extremities; therefore, we consider that the temperature of the pore fluid entering and exiting the sample was the same as the sample temperature. Once the maximum desired temperature was reached and permeability at that temperature was measured, samples were cooled at either 10°C/min or 20°C/min to ambient laboratory temperatures. All permeability measurements were made under a confining pressure,  $P_c$ , of 50 MPa; the effective pressure,  $P_{\text{eff}} = P_c - P_m$ , on the sample was approximately 49 MPa for all measurements.

To measure permeability under steady state flow conditions, a constant pore fluid pressure,  $P_u$ , was applied upstream of the sample and monitored using a pressure gauge.  $P_d$  was atmospheric pressure. Permeability was determined by increasing  $P_u$  and recording the stabilized  $Q_v$  for each  $P_u$  increment. The permeability of all samples was corrected for the effect of temperature on volumetric flow and, if necessary, the Forchheimer (Forchheimer, 1901) and Klinkenberg (Klinkenberg, 1941) effects (see supporting information).

To verify our methodology, we confirm the experimental efficacy of equation (4) by measuring the permeability of a ceramic standard (74% Al<sub>2</sub>O<sub>3</sub> + SiO<sub>2</sub> Umicore mullite ceramic) as a function of temperature. The coefficient of thermal expansion of the ceramic is  $5 \times 10^{-6}/^\circ\text{C}$  (resulting in a total volumetric expansion of only 0.4 vol % at 800°C) and the material shows no structural degradation up to 1,200°C (Latella et al., 2006), thus, the permeability of the ceramic should remain constant up to 800°C. The permeability of the mullite ceramic was measured at five different temperatures: 25, 200, 400, 600, and 800°C (Table S1); permeability measurements at 25°C and 200°C were performed at the end of the heating cycle to ensure that there was sufficient coupling between the iron jacket and the sample. The error on the permeability measurements is  $\pm 3.5\%$ .

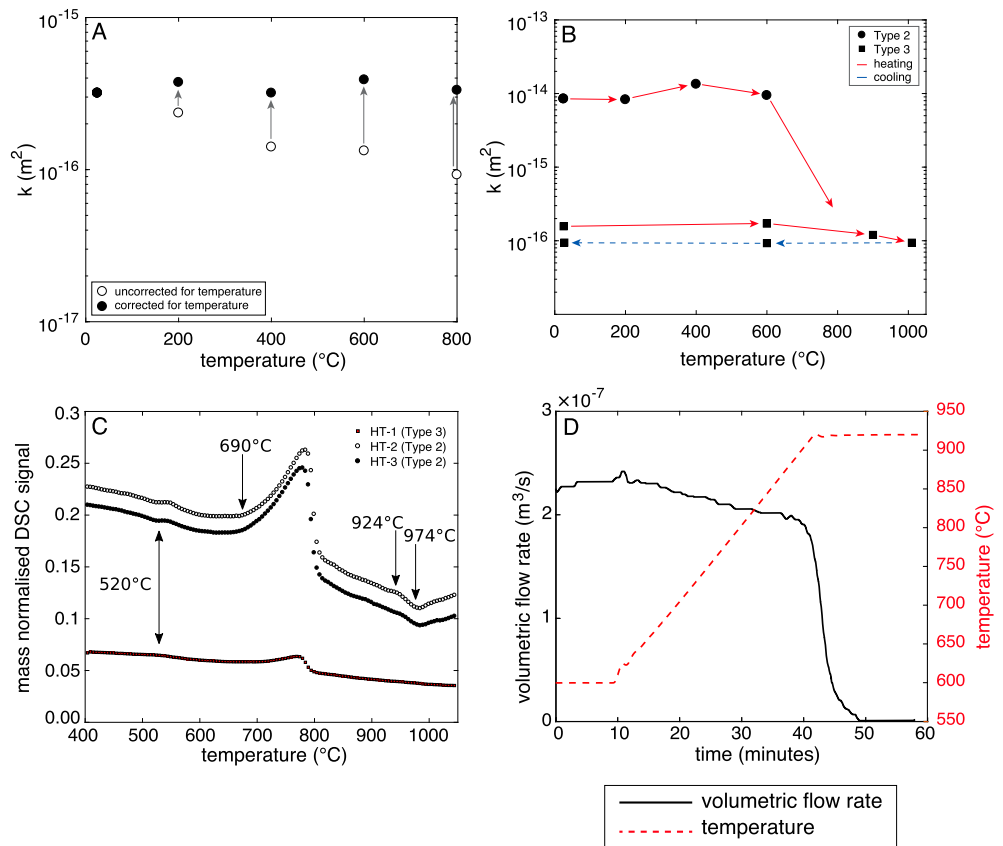


**Figure 1.** Permeability, differential scanning calorimetry, and volumetric flow rate response to increasing temperature in basaltic andesite. (a) Permeability of the mullite ceramic standard. Unfilled circles—uncorrected for the effect of temperature on the density of the pore fluid. Black circles—corrected for the effect of temperature on the density of the pore fluid. (b) Permeability of Type 2 (HT-4) and Type 3 (HT-1) basaltic andesites from Merapi. All values are corrected for the Forchheimer and Klinkenberg effects as indicated in Table S1, as well as for the effect of temperature on the density of the pore fluid. The error on all measurements lies within the symbol size. (c) Differential scanning calorimetry of the Types 2 and 3 basaltic andesites. (d). Volumetric flow rate,  $Q_v$ , and temperature evolution through time for HT-2. The sample permeability falls below  $10^{-19}$  m<sup>2</sup> between 900 and 920°C over approximately 8 min.

Before accounting for the change in argon density as a result of temperature, the permeability of the ceramic standard appears to decrease with increasing temperature (Figure 1a). However, when the change in argon density is taken into consideration, this decreasing trend is absent. This confirms that all volumetric flow rate data gathered at elevated temperature must be corrected for the change in pore fluid density before changes in permeability can be assessed as a function of temperature.

#### 4. Materials: Basaltic Andesites From Merapi, Indonesia

We measured the permeability of two different types of basaltic andesite sampled from the deposits of the 2010 eruption of Merapi (Indonesia) for which the permeability-microtexture relationships have been previously described by Kushnir et al. (2016). Type 2 basaltic andesites are scoriaceous to blocky in hand sample and are the eruptive products of the juvenile magma produced and extruded during the course of the 2010 eruption. The permeability in these samples is vesicle- and fracture-controlled, and the relative importance of these void space geometries changes with connected porosity; in scoriaceous samples, vesicles exert a more important control on permeability than in the more dense blocks, though permeability is fundamentally controlled by the fractures that connect these pores (Figure 2a). Type 3 basaltic andesites represent the dome rocks emplaced at the end of the previous eruption and are relatively glass-poor compared to the Type 2 rocks. The permeability of these rocks is dominantly fracture controlled but is also influenced by diktytaxitic textures (Figure 2b).

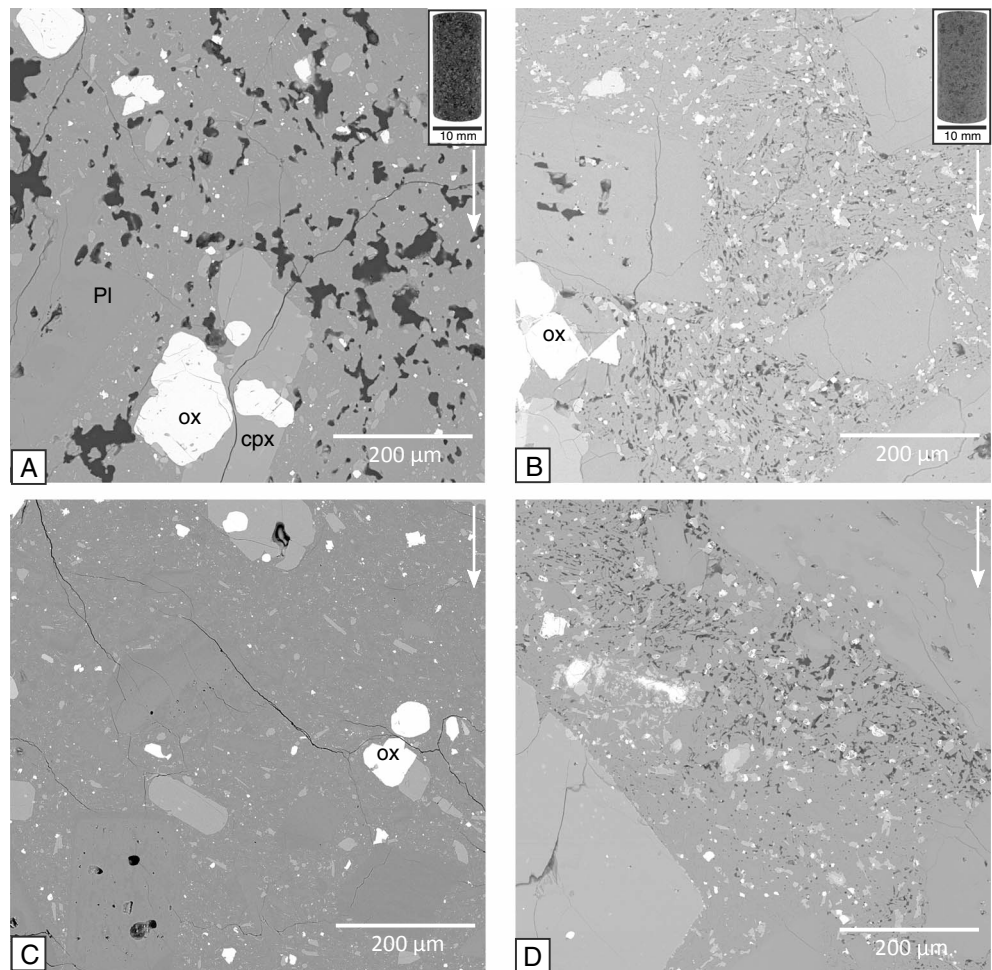


**Figure 2.** Preheating and postheating microstructure. Scanning electron microscope (SEM) backscattered electron images of the microstructure of the Type 2 and Type 3 basaltic andesites from Merapi. The white arrows denote the direction of fluid flow during permeability measurements. Microstructure of the starting material, before heating: (a) Type 2. (b) Type 3. Microstructure after high temperature permeability measurements: (c) Type 2. (d) Type 3. Ox = oxides, cpx = clinopyroxene.

Differential scanning calorimetry (DSC; see Heap et al., 2017 for measurement details) of the Type 2 and Type 3 basaltic andesites heated at 25°C/min show the onset of a calorimetric glass transition at 520°C (Figure 1c). We note that the Type 3 rock contains only trace glass phase and the DSC peak is small but present. This glass transition temperature is consistent with an H<sub>2</sub>O content of 1.1 wt % (we derived the viscosities using Giordano et al., 2008 and the average glass composition given by Erdmann et al., 2016 and Preece et al., 2016). In all samples, the glass transition peak is followed by a large endothermic peak beginning at 690°C that is associated with a large mass loss event (shown by thermogravimetric analysis, see Figure S6). This peak likely reflects the loss of dissolved magmatic water (Giachetti et al., 2015). In Type 2 samples, the onset of a crystallization exotherm occurs at 974°C, preceded by a small endothermic peak at 924°C, possibly related to a second boiling event. All reported permeability measurements were conducted at temperatures below or in excess of the observed mass loss event between 690°C and 800°C—attributed to a loss of magmatic water from the system—ensuring that the mass of pore fluid entering and exiting the sample was conserved.

## 5. Results

In this study, we measured the permeability of one Type 3 sample (HT-1) and three Type 2 samples (HT-2, HT-3, and HT-4); sample details and permeability data are given in Table S1. Sample HT-1 (Type 3)

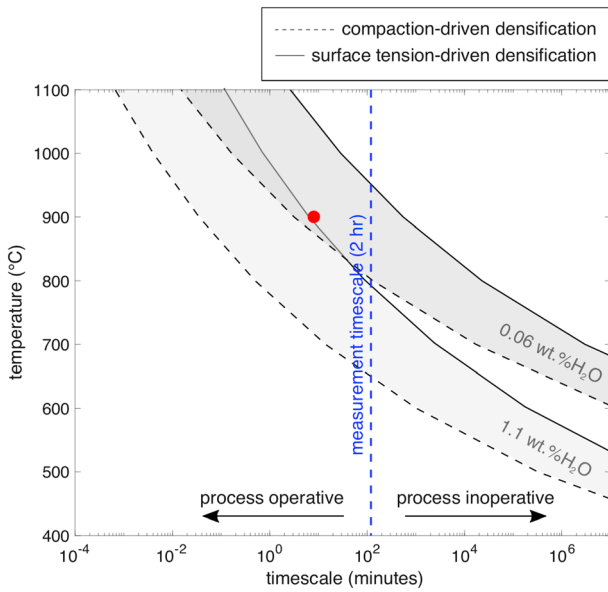


**Figure 3.** Timescales of compaction-driven,  $\tau_c$ , and surface tension-driven,  $\tau_t$ , densification.  $\tau_c$  and  $\tau_t$  are calculated using the glass composition of the basaltic andesites used in this study for water contents of 1.1 and 0.06 wt %. The time taken for each permeability measurement,  $\tau$ , is denoted by the blue dashed line. Processes operative and observable over  $\tau$  are to the left of the blue dashed line. The time taken for permeability shut-off in samples HT-2 and HT-3 is denoted by the red dot.

remained permeable throughout heating and cooling (Figure 1b), though its permeability decreased by  $8 \times 10^{-17} \pm 7 \times 10^{-18} \text{ m}^2$  above 900°C (this represents a fractional change in permeability of only 0.02). Upon cooling, the permeability of this sample did not change. The overall microstructure of the Type 3 basaltic andesite remained notably unchanged up to  $T = 1,010^\circ\text{C}$  (Figure 2d): we see no qualitative change in fracture density and the diktytaxitic textures remain preserved.

The permeability of samples HT-2 and HT-3 (both Type 2) fell below  $10^{-19} \text{ m}^2$  (the minimum permeability that can be measured in our system) above 900°C, as demonstrated by the decrease of  $Q_v$  to 0 mL/min (Figure 1d). Both samples were cooled once  $Q_v$  decayed to 0 mL/min; neither sample became permeable during cooling. In thin section, we note that Type 2 samples experienced a significant reduction of the area fraction of vesicles after being heated above 900°C, though some through-going fractures remained (Figure 2c).

The permeability of sample HT-4 remained constant up to 600°C, with a small increase noted at 400°C (Figure 1b); this excursion is within the variance of the measurements. At 800°C, the sample experienced a decrease in permeability of  $\sim 2$  orders of magnitude to  $10^{-16} \text{ m}^2$ . The permeability of this sample did not stabilize at 800°C but continued to decrease with time, reflecting an unstable microstructure. Since the microstructure did not stabilize over the course of the measurement, the sample was cooled to room temperature. Permeability remained constant during cooling (Table S1).

## 6. Discussion

All samples in this study experienced a decrease in permeability at temperatures above 800°C. The permeability of these samples is controlled by the connectivity of a pore-fracture microstructure; therefore, permeability reduction was dependent on the efficiency of the closure of these features. To assess the dominant processes in the densification of our samples, we consider the surface tension timescale and the timescale of stress-induced compaction (Kennedy et al., 2016). The surface tension timescale, which is responsible for the collapse of pore space due to surface tension forces, is defined as  $\tau_t = R\eta_m/\Gamma$ , where  $R$  is the pore radius,  $\eta_m$  is the melt viscosity, and  $\Gamma$  is the surface tension of a hydrous melt, taken to be 0.07 N/m (Gardner & Ketcham, 2011). The compaction timescale, which defines the timescale for stress-driven compaction, is defined as  $\tau_c = \eta_s/\sigma$ , where  $\sigma$  is the applied stress on the sample (Sparks et al., 1999).  $\eta_s = \eta_m(1 - \Phi/\Phi_m)^{-2}$ , where  $\eta_m$  is the melt viscosity,  $\Phi$  is the crystal fraction of the sample, and  $\Phi_m$  is the maximum closed packing fraction for crystals (Maron & Pierce, 1956). For a suspension of particles consistent with typical phenocryst and microlite aspect ratios, we assume a  $\Phi_m$  of 0.538 (Mueller et al., 2011). In this study,  $\sigma = P_{\text{eff}} = 49 \text{ MPa}$  and  $\Phi = 0.5$ .

We compare  $\tau_t$  and  $\tau_c$  for each target temperature, assuming an H<sub>2</sub>O content of 1.1 wt % and a pore radius of 50  $\mu\text{m}$ , consistent with the pore sizes observed in HT-3 and HT-4 (Table S3 and Figure 3). We find that in our system compaction under the effective stress dominates; however, above 700°C, this timescale is much shorter than the time spent at any of the temperature steps (<2 h; Figure 3).

In this study,  $P_m$  did not exceed 1 MPa. Further, because the pore fluid was argon, the partial pressure of H<sub>2</sub>O in the permeable network was significantly lower than 1 MPa resulting in a pressure gradient capable of driving H<sub>2</sub>O diffusion from the melt filaments (at  $P_c = 50 \text{ MPa}$ ) to the pore space, consequently increasing the melt viscosity over time. At 600°C and an initial water content of 1.1 wt %, the diffusivity of total water in rhyolitic liquids,  $D_T$ , is  $2.26 \times 10^{-13} \text{ m}^2 \text{ s}^{-1}$  (Zhang & Ni, 2010). The timescale required for thorough diffusion can be approximated by  $\lambda_D = l^2/D_T$ . In our experiments, the length scale,  $l$ , of the interpore distances is between 20 and 100  $\mu\text{m}$ , confirmed using scanning electron microscope (SEM) imaging and the time required to completely degas the interpore filaments at 600°C is between 29 and 736 min. While the upper limit of this timescale

is longer than the time spent at 600°C ( $\approx 120$  min), melt dehydration was a continuous process and resulted in complete melt dehydration by 800°C, consistent with the mass loss event observed by DSC. We conclude that the dissolved water contained in the melt was reduced significantly before the timescale of compaction became comparable to the measurement length and assume a low equilibrium water content of 0.06 wt % in our estimation of melt viscosity. At 900°C, the timescale of relaxation for compaction is approximately 3 min (Table S3), which is consistent with the timescale over which we observe permeability reduction in our experiments (Figure 3). Therefore, permeability reduction in our system is controlled by stress-induced viscous compaction of the pore network. We highlight that since the measurements were conducted under hydrostatic conditions, compaction was uniform in all directions.

While the permeability of the Type 3 basaltic andesite (HT-1) decreased above 900°C, the sample remained permeable up to 1,010°C; this is explained by the negligible mass fraction of glass within the sample. Without significant glassy components to be remobilized at high temperature, the microstructure could not viscously relax and the permeability of this rock remained largely unchanged. We note that the use of an argon pore fluid in the present study precludes dissolution/precipitation mechanisms that act to reduce permeability in other high temperature permeability studies (Moore et al., 1994; Morrow et al., 2001; Summers et al., 1978).

The heating rates used in this study are expected to incite thermal expansion of crystals and thermally induced cracking (Richter & Simmons, 1974), which may modify the sample microstructure of the basaltic andesites; however, we see no evidence in the permeability data to suggest this. By contrast, a decrease in permeability of nearly four orders of magnitude up to 800°C has been observed in spine-forming dacites from Mount St. Helens (MSH), USA (Figure S7). This overall decrease in permeability has been attributed to competing micromechanisms during heating, including thermal expansion of crystals, thermally induced microcracking, rock-water chemical healing, and crystal plasticity (Gaunt et al., 2016). However, Gaunt et al. (2016) do not account for the change in density of the water pore fluid between the hot sample and the significantly cooler fluid reservoirs. We note that when the Mount St Helens data are corrected for the effect of temperature on the density of water, the change in permeability becomes less than 2 orders of magnitude (Figure S7). The connected porosity of the MSH dacite used in that study amounted to only 0.06, and permeability was fracture controlled. With a crystal fraction of nearly 1, reactivation of any residual glass phase with increasing temperature was not operative in modifying the overall rock permeability and, thus, permeability reduction was sensitive to fracture closure due to thermal expansion of crystals. While thermal cracking in those rocks acted to combat permeability decrease, water-facilitated precipitation-driven crack sealing acted to further reduce permeability at  $T < 600^\circ\text{C}$ . We conclude that the microstructural changes proposed by Gaunt et al. (2016) do very little to modify the permeability of the samples in the present study. Indeed, permeability of our volcanic materials is largely unaffected by changes in temperature below the calorimetric glass transition. However, once the melt viscosity is sufficiently lowered, the onset of permeability reduction and shutoff is rapid, suggesting an efficient process with profound consequences.

Conduit reheating and sealing is a physically feasible process that has been identified at rhyolite-basalt interfaces (Kennedy et al., 2010; Schaubroth et al., 2016). While we conclude that a significant increase in temperature is unlikely to result in a pronounced modification to the permeability of a devitrified volcanic dome between eruption cycles, remobilization of any residual glass phase both in the edifice and at conduit margins remains a compelling process for drastic and efficient permeability reduction. Sufficient reheating of glassy samples triggers porosity collapse and fracture healing, the rate of which is dependent on the amount by which  $T_g$  is surpassed (Okumura & Sasaki, 2014). Indeed, at Merapi, magma storage and pre-eruptive recharge temperatures were between 925 and 1,000°C prior to the 2010 eruption (Erdmann et al., 2016); such temperatures are high enough to remobilize the glass phase of the juvenile samples used in this study, which may have resulted in thermally induced sealing of the permeable network. This process of reheating and relaxation remains a potential mechanism for sealing at conduit margins (Heap et al., 2017; Kennedy et al., 2010; Schaubroth et al., 2016), inhibiting volatile escape to the surrounding edifice and contributing to gas overpressures that may tax the volcanic plumbing at depth. However, we emphasize that this process will undoubtedly be accompanied by other processes that significantly alter permeability including deformation (Farquharson et al., 2016; Heap et al., 2017; Kushnir et al., 2017; Laumonier et al., 2011; Lavallée et al., 2013; Okumura et al., 2010, 2009; Violay et al., 2015) and the deposition of vapor transported phases (Baxter et al., 1999; de Hoog et al., 2005; Wright et al., 2011).

## 7. Conclusions

So-called in situ—under high-temperature and/or high-pressure conditions—permeability measurements permit us to begin to characterize the processes attending permeability development in magmas in the absence of microstructural overprinting that inevitably accompanies the emplacement of volcanic rocks. We emphasize that a correction for the change in pore fluid density between the sample (which controls permeability) and the pore volume reservoirs (where volumetric flow rate is measured) must be applied when assessing the permeability of rock samples measured at high temperature.

A simple case study of the permeability of glassy and glass-poor basaltic andesites from Merapi suggests that permeability is largely insensitive to temperature until the calorimetric glass transition of the glass phase is exceeded and the viscosity of the crystal suspension is reduced sufficiently to accommodate any applied stresses. The microstructure of these samples is consistent with a sequence of processes: (i) viscous relaxation of the interstitial glass, (ii) resulting in a loss of competence of the material, and (iii) viscous compaction under the elevated effective pressure. The resultant porosity loss causes the permeable network to seal, effectively curtailing fluid flow. However, an increase in temperature up to 1,010°C does not significantly alter the permeability of the Type 3 basaltic andesite owing to the distinct lack of interstitial glass. Thus, any significant reduction in permeability in response to high temperature requires the presence of a glass phase that can be sufficiently remobilized to seal preexisting gas pathways, facilitating overpressure development within the volcanic edifice.

## Acknowledgments

This work was funded in part by the Agence Nationale de la Recherche (ANR) project DOMERAPI (ANR-12-BS06-0012). A. R. L. K. acknowledges a Postgraduate Scholarship-Doctoral (CGSD3-444207-2013) provided by the Natural Sciences and Engineering Research Council of Canada (NSERC). The authors would like to thank T. Reuschlé, J. I. Farquharson, and M. J. Heap for helpful discussions. I. Di Carlo are thanked for SEM assistance and Q. Thibault, E. Le Moing, F. Savoie, and R. Planckaert is thanked for technical assistance. This manuscript benefited from the constructive reviews of M. Violay and an anonymous reviewer. All data can be found in the supporting information.

## References

- Bakker, R. R., Violay, M. E. S., Benson, P. M., & Vinciguerra, S. C. (2015). Ductile flow in sub-volcanic carbonate basement as the main control for edifice stability: New experimental insights. *Earth and Planetary Science Letters*, *430*, 533–541. <https://doi.org/10.1016/j.epsl.2015.08.017>
- Baxter, P. J., Bonadonna, C., Dupree, R., Hards, V. L., Kohn, S. C., Murphy, M. D., ... Vickers, B. P. (1999). Cristobalite in volcanic ash of the Soufriere Hills volcano, Montserrat, British West Indies. *Science*, *283*(5405), 1142–1145. <https://doi.org/10.1126/science.283.5405.1142>
- Bernard, M.-L., Zomara, M., Géraud, Y., & Boudon, G. (2007). Transport properties of pyroclastic rocks from Montagne Pelée volcano (Martinique, Lesser Antilles). *Journal of Geophysical Research*, *112*, B05205. <https://doi.org/10.1029/2006JB004385>
- Coelho, G., Branquet, Y., Sizaret, S., Arbaret, L., Champallier, R., & Rozenbaum, O. (2015). Permeability of sheeted dykes beneath oceanic ridges: Strain experiments coupled with 3D numerical modeling of the Troodos ophiolite, Cyprus. *Tectonophysics*, *644–645*, 138–150. <https://doi.org/10.1016/j.tecto.2015.01.004>
- Collinson, A. S. D., & Neuberg, J. W. (2012). Gas storage, transport and pressure changes in an evolving permeable volcanic edifice. *Journal of Volcanology and Geothermal Research*, *243*, 1–13. <https://doi.org/10.1016/j.jvolgeores.2012.06.027>
- Collombet, M. (2009). Two-dimensional gas loss for silicic magma flows: Toward more realistic numerical models. *Geophysical Journal International*, *177*(1), 309–318. <https://doi.org/10.1111/j.1365-246X.2008.04086.x>
- de Hoog, J. C. M., van Bergen, M. J., & Jacobs, M. H. G. (2005). Vapour-phase crystallisation of silica from SiF<sub>4</sub>-bearing volcanic gases. *Annals of Geophysics*, *48*(4–5), 775–785.
- Eichelberger, J. C., Carrigan, C. R., Westrich, H. R., & Price, R. H. (1986). Non-explosive silicic volcanism. *Nature*, *323*(6089), 598–602. <https://doi.org/10.1038/323598a0>
- Erdmann, S., Martel, C., Pichavant, M., Bourdier, J. L., Champallier, R., Komorowski, J. C., & Cholik, N. (2016). Constraints from phase equilibrium experiments on pre-eruptive storage conditions in mixed magma systems: A case study on crystal-rich basaltic Andesites from mount Merapi, Indonesia. *Journal of Petrology*, *57*(3), 535–560. <https://doi.org/10.1093/petrology/egw019>
- Farquharson, J., Heap, M. J., Varley, N. R., Baud, P., & Reuschlé, T. (2015). Permeability and porosity relationships of edifice-forming andesites: A combined field and laboratory study. *Journal of Volcanology and Geothermal Research*, *297*, 52–68. <https://doi.org/10.1016/j.jvolgeores.2015.03.016>
- Farquharson, J. I., Heap, M. J., & Baud, P. (2016). Strain-induced permeability increase in volcanic rock. *Geophysical Research Letters*, *43*(22), 11,603–11,610. <https://doi.org/10.1002/2016GL071540>
- Fischer, G. J., & Paterson, M. S. (1992). The determination of permeability and storage capacity: Pore pressure oscillation method. In B. Evans & T.-F. Wong (Eds.), *Fault mechanics and transport properties of rocks* (Chap. 9, pp. 213–252). San Diego, CA: International Geophysics.
- Forchheimer, P. (1901). Water movement through ground. *Zeitschrift Des Vereines Deutscher Ingenieure*, *45*, 1736–1741.
- Frost, H. J., & Ashby, M. F. (1982). *Deformation-Mechanism Maps: The Plasticity and Creep of Metals and Ceramics*. Oxford: Pergamon Press.
- Gardner, J. E., & Ketchum, R. A. (2011). Bubble nucleation in rhyolite and dacite melts: Temperature dependence of surface tension. *Contributions to Mineralogy and Petrology*, *162*(5), 929–943. <https://doi.org/10.1007/s00410-011-0632-5>
- Gaunt, H. E., Sammonds, P. R., Meredith, P. G., Smith, R., & Pallister, J. S. (2014). Pathways for degassing during the lava dome eruption of Mount St. Helens 2004–2008. *Geology*, *42*(11), 947–950. <https://doi.org/10.1130/G35940.1>
- Gaunt, H. E., Sammonds, P. R., Meredith, P. G., & Chadderton, A. (2016). Effect of temperature on the permeability of lava dome rocks from the 2004–2008 eruption of Mount St. Helens. *Bulletin of Volcanology*, *78*(4). <https://doi.org/10.1007/s00445-016-1024-5>
- Giachetti, T., Gonnermann, H. M., Gardner, J. E., Shea, T., & Gouldstone, A. (2015). Discriminating secondary from magmatic water in rhyolitic matrix-glass of volcanic pyroclasts using thermogravimetric analysis. *Geochimica et Cosmochimica Acta*, *148*, 457–476. <https://doi.org/10.1016/j.gca.2014.10.017>
- Giordano, D., Russell, J. K., & Dingwell, D. B. (2008). Viscosity of magmatic liquids: A model. *Earth and Planetary Science Letters*, *271*(1–4), 123–134. <https://doi.org/10.1016/j.epsl.2008.03.038>
- Heap, M. J., Farquharson, J. I., Baud, P., Lavallée, Y., & Reuschlé, T. (2015). Fracture and compaction of andesite in a volcanic edifice. *Bulletin of Volcanology*, *77*(6), 55. <https://doi.org/10.1007/s00445-015-0938-7>

- Heap, M. J., Violay, M., Wadsworth, F. B., & Vasseur, J. (2017). From rock to magma and back again: The evolution of temperature and deformation mechanism in conduit margin zones. *Earth and Planetary Science Letters*, *463*, 92–100. <https://doi.org/10.1016/j.epsl.2017.01.021>
- Jaupart, C. (1998). Gas loss from magmas through conduit walls during eruption. In J. S. Gilbert & R. S. J. Sparks (Eds.), *The physics of explosive volcanic eruptions* (pp. 73–90). London: Geological Society.
- Jaupart, C., & Allegre, C. J. (1991). Gas content, eruption rate and instabilities of eruption regime in silicic volcanos. *Earth and Planetary Science Letters*, *102*(3–4), 413–429. [https://doi.org/10.1016/0012-821X\(91\)90032-D](https://doi.org/10.1016/0012-821X(91)90032-D)
- Kennedy, B. M., Jellinek, A. M., Russell, J. K., Nichols, A. R. L., & Vigouroux, N. (2010). Time- and temperature-dependent conduit wall porosity: A key control on degassing and explosivity at Tarawera volcano, New Zealand. *Earth and Planetary Science Letters*, *299*(1–2), 126–137. <https://doi.org/10.1016/j.epsl.2010.08.028>
- Kennedy, B. M., Wadsworth, F. B., Vasseur, J., Ian Schipper, C., Mark Jellinek, A., von Aulock, F. W., ... Dingwell, D. B. (2016). Surface tension driven processes densify and retain permeability in magma and lava. *Earth and Planetary Science Letters*, *433*, 116–124. <https://doi.org/10.1016/j.epsl.2015.10.031>
- Klinkenberg, L. J. (1941). The permeability of porous media to liquids and gases. *Drilling and Production Practice*, 200–213.
- Klug, C., & Cashman, K. V. (1996). Permeability development in vesiculating magmas: Implications for fragmentation. *Bulletin of Volcanology*, *58*(2–3), 87–100. <https://doi.org/10.1007/s004450050128>
- Kushnir, A. R. L., Martel, C., Bourdier, J. L., Heap, M. J., Reuschlé, T., Erdmann, S., ... Cholik, N. (2016). Probing permeability and microstructure: Unravelling the role of a low-permeability dome on the explosivity of Merapi (Indonesia). *Journal of Volcanology and Geothermal Research*, *316*, 56–71. <https://doi.org/10.1016/j.jvolgeores.2016.02.012>
- Kushnir, A. R. L., Martel, C., Champallier, R., & Arbaret, L. (2017). In Situ Confirmation of Permeability Development in Shearing Bubble-Bearing Melts and Implications for Volcanic Outgassing. *Earth and Planetary Science Letters*, *458*, 315–326. <https://doi.org/10.1016/j.epsl.2016.10.053>
- Latella, B. A., Henkel, L., & Mehrtens, E. G. (2006). Permeability and high temperature strength of porous mullite-alumina ceramics for hot gas filtration. *Journal of Materials Science*, *41*(2), 423–430. <https://doi.org/10.1007/s10853-005-2654-8>
- Laumonier, M., Arbaret, L., Burgisser, A., & Champallier, R. (2011). Porosity redistribution enhanced by strain localization in crystal-rich magmas. *Geology*, *39*(8), 715–718. <https://doi.org/10.1130/G31803.1>
- Lavallée, Y., Benson, P. M., Heap, M. J., Hess, K. U., Flaws, A., Schillinger, B., ... Dingwell, D. B. (2013). Reconstructing magma failure and the degassing network of dome-building eruptions. *Geology*, *41*(4), 515–518. <https://doi.org/10.1130/G33948.1>
- Maron, S. H., & Pierce, P. E. (1956). Application of Ree-Eyring generalized flow theory to suspensions of spherical particles. *Journal of Colloid Science*, *11*, 80–95.
- Moore, D. E., Lockner, D. A., & Byerlee, J. D. (1994). Reduction of permeability in granite at elevated-temperatures. *Science*, *265*(5178), 1558–1561. <https://doi.org/10.1126/science.265.5178.1558>
- Morrow, C., Lockner, D., Moore, D., & Byerlee, J. (1981). Permeability of granite in a temperature-gradient. *Journal of Geophysical Research*, *86*(B4), 3002–3008. <https://doi.org/10.1029/JB086iB04p03002>
- Morrow, C. A., Moore, D. E., & Lockner, D. A. (2001). Permeability reduction in granite under hydrothermal conditions. *Journal of Geophysical Research*, *106*(B12), 30551–30560. <https://doi.org/10.1029/2000JB000010>
- Mueller, S., Llewellyn, E. W., & Mader, H. M. (2011). The effect of particle shape on suspension viscosity and implications for magmatic flows. *Geophysical Research Letters*, *38*, L13316. <https://doi.org/10.1029/2011GL047167>
- Mueller, S., Scheu, B., Spieler, O., & Dingwell, D. B. (2008). Permeability control on magma fragmentation. *Geology*, *36*(5), 399–402. <https://doi.org/10.1130/G24605A.1>
- Okumura, S., & Sasaki, O. (2014). Permeability reduction of fractured rhyolite in volcanic conduits and its control on eruption cyclicity. *Geology*, *42*(10), 843–846. <https://doi.org/10.1130/G35855.1>
- Okumura, S., Nakamura, M., & Tsuchiyama, A. (2006). Shear-induced bubble coalescence in rhyolitic melts with low vesicularity. *Geophysical Research Letters*, *33*, L20316. <https://doi.org/10.1029/2006GL027347>
- Okumura, S., Nakamura, M., Tsuchiyama, A., Nakano, T., & Uesugi, K. (2008). Evolution of bubble microstructure in sheared rhyolite: Formation of a channel-like bubble network. *Journal of Geophysical Research*, *113*, B07208. <https://doi.org/10.1029/2007JB005362>
- Okumura, S., Nakamura, M., Takeuchi, S., Tsuchiyama, A., Nakano, T., & Uesugi, K. (2009). Magma deformation may induce non-explosive volcanism via degassing through bubble networks. *Earth and Planetary Science Letters*, *281*(3–4), 267–274. <https://doi.org/10.1016/j.epsl.2009.02.036>
- Okumura, S., Nakamura, M., Nakano, T., Uesugi, K., & Tsuchiyama, A. (2010). Shear deformation experiments on vesicular rhyolite: Implications for brittle fracturing, degassing, and compaction of magmas in volcanic conduits. *Journal of Geophysical Research*, *115*, B06201. <https://doi.org/10.1029/2009JB006904>
- Preece, K., Gertisser, R., Barclay, J., Charbonnier, S. J., Komorowski, J. C., & Herd, R. A. (2016). Transitions between explosive and effusive phases during the cataclysmic 2010 eruption of Merapi volcano, Java, Indonesia. *Bulletin of Volcanology*, *78*(8). <https://doi.org/10.1007/s00445-016-1046-z>
- Richter, D., & Simmons, G. (1974). Thermal expansion behaviour of igneous rocks. *International Journal of Rock Mechanics and Mining Sciences*, *11*(10), 403–411. [https://doi.org/10.1016/0148-9062\(74\)91111-5](https://doi.org/10.1016/0148-9062(74)91111-5)
- Rust, A. C., & Cashman, K. V. (2004). Permeability of vesicular silicic magma: Inertial and hysteresis effects. *Earth and Planetary Science Letters*, *228*(1–2), 93–107. <https://doi.org/10.1016/j.epsl.2004.09.025>
- Rust, A. C., Cashman, K. V., & Wallace, P. J. (2004). Magma degassing buffered by vapor flow through brecciated conduit margins. *Geology*, *32*(4), 349–352. <https://doi.org/10.1130/G20388.2>
- Saar, M. O., & Manga, M. (1999). Permeability-porosity relationship in vesicular basalts. *Geophysical Research Letters*, *26*(1), 111–114. <https://doi.org/10.1029/1998GL900256>
- Schauthroth, J., Wadsworth, F. B., Kennedy, B., von Aulock, F. W., Lavallée, Y., Damby, D. E., ... Dingwell, D. B. (2016). Conduit margin heating and deformation during the AD 1886 basaltic Plinian eruption at Tarawera volcano, New Zealand. *Bulletin of Volcanology*, *78*(2), 12. <https://doi.org/10.1007/s00445-016-1006-7>
- Siebert, L. (1984). Large volcanic debris avalanches: Characteristics of source areas, deposits, and associated eruptions. *Journal of Volcanology and Geothermal Research*, *22*(3–4), 163–197. [https://doi.org/10.1016/0377-0273\(84\)90002-7](https://doi.org/10.1016/0377-0273(84)90002-7)
- Sparks, R. S. J., Tait, S. R., & Yanev, Y. (1999). Dense welding caused by volatile resorption. *Journal of the Geological Society*, *156*(2), 217–225. <https://doi.org/10.1144/gsjgs.156.2.0217>
- Stasiuk, M. V., Barclay, J., Carroll, M. R., Jaupart, C., Ratte, J. C., Sparks, R. S. J., & Tait, S. R. (1996). Degassing during magma ascent in the Mule Creek vent (USA). *Bulletin of Volcanology*, *58*(2–3), 117–130. <https://doi.org/10.1007/s004450050130>

- Summers, R., Winkler, K. W., & Byerlee, J. (1978). Permeability changes during the flow of water through westerly granite at temperatures of 1000°–400°C. *Journal of Geophysical Research*, 83(B1), 339–344. <https://doi.org/10.1029/JB083iB01p00339>
- Thomas, M. E., & Neuberg, J. (2012). What makes a volcano tick—a first explanation of deep multiple seismic sources in ascending magma. *Geology*, 40(4), 351–354. <https://doi.org/10.1130/G32868.1>
- Tuffen, H., & Dingwell, D. (2005). Fault textures in volcanic conduits: Evidence for seismic trigger mechanisms during silicic eruptions. *Bulletin of Volcanology*, 67(4), 370–387. <https://doi.org/10.1007/s00445-004-0383-5>
- Vinciguerra, S., Trovato, C., Meredith, P. G., & Benson, P. M. (2005). Relating seismic velocities, thermal cracking and permeability in Mt. Etna and Iceland basalts. *International Journal of Rock Mechanics and Mining Sciences*, 42(7–8), 900–910. <https://doi.org/10.1016/j.ijmms.2005.05.022>
- Violay, M., Gibert, B., Mainprice, D., & Burg, J. P. (2015). Brittle versus ductile deformation as the main control of the deep fluid circulation in oceanic crust. *Geophysical Research Letters*, 42, 2767–2773. <https://doi.org/10.1002/2015GL063437>
- Watanabe, N., Numakura, T., Sakaguchi, K., Saishu, H., Okamoto, A., Ingebritsen, S. E., & Tsuchiya, N. (2017). Potentially exploitable supercritical geothermal resources in the ductile crust. *Nature Geoscience*, 10(2), 140–145. <https://doi.org/10.1038/ngeo2879>
- Woods, A. W., & Koyaguchi, T. (1994). Transitions between explosive and effusive eruptions of silicic magmas. *Nature*, 370(6491), 641–644. <https://doi.org/10.1038/370641a0>
- Wright, H. M. N., Cashman, K. V., Gottesfeld, E. H., & Roberts, J. J. (2009). Pore structure of volcanic clasts: Measurements of permeability and electrical conductivity. *Earth and Planetary Science Letters*, 280(1–4), 93–104. <https://doi.org/10.1016/j.epsl.2009.01.023>
- Wright, H. M. N., Lesti, C., Cas, R. A. F., Porreca, M., Viramonte, J. G., & Giordano, G. (2011). Columnar jointing in vapour-phase-altered, non-welded Cerro Galán ignimbrite, Paycuqui, Argentina. *Bulletin of Volcanology*, 73(10), 1567–1582. <https://doi.org/10.1007/s00445-011-0524-6>
- Zhang, Y., & Ni, H. (2010). Diffusion of H, C, and O components in silicate melts. *Diffusion in Minerals and Melts*, 72, 171–225.
- Zharikov, A. V., Vitovtova, V. M., Shmonov, V. M., & Grafchikov, A. A. (2003). Permeability of the rocks from the kola superdeep borehole at high temperature and pressure: Implication to fluid dynamics in the continental crust. *Tectonophysics*, 370(1–4), 177–191. [https://doi.org/10.1016/S0040-1951\(03\)00185-9](https://doi.org/10.1016/S0040-1951(03)00185-9)